Supporting Information for "Correlation Between Cloud Adjustments and Cloud Feedbacks Responsible for Larger Range of Climate Sensitivities in CMIP6"

N. J. Lutsko[1], M. T. Luongo[1], C. J. Wall[1], T. A. Myers[23]

Contents of this file

Corresponding author: N. J. Lutsko, Scripps Institution of Oceanography, University of California at San Diego, La Jolla, California (nlutsko@ucsd.edu)

[1]Scripps Institution of Oceanography, University of California at San Diego, La Jolla, California.

[2]Cooperative Institute for Research in Environmental Sciences (CIRES), University of Colorado, Boulder, Colorado, USA

[3]Physical Science Laboratory, National Oceanic and Atmospheric Administration, Boulder, Colorado, USA

1. Text S1

2. Figures S1 and S2

Introduction The supplementary material contains a description of the Cloud Controlling Factor analysis in test S1 and two figures. Figure S1 compares different methods of estimating radiative forcing in CMIP5 and CMIP6. Figure S2 breaks down the different components of the Cloud Controlling Factor analysis.

Text S1. Cloud Controling Factor Analysis To investigate how changes in governing meteorological conditions contribute to low cloud adjustments, we perform a cloud controlling factor (CCF) analysis [e.g., *Klein et al.*, 2018; *Scott et al.*, 2020]. The basic assumption of a CCF analysis is that the change in some property of low clouds, for example the low cloud radiative effect, R, in response to a forcing (Δ, taken here to be abrupt 4xCO2 forcing), can be represented as a first-order Taylor expansion in CCFs, x_i:

$$\Delta R = \sum_i \frac{\partial R}{\partial x_i} \Delta x_i. \tag{1}$$

Above, the partial derivatives are the sensitivity of R to respective CCFs (i.e. meteorological cloud radiative kernels) and are assumed to be time-scale invariant. The Δx_i terms are the change in the CCF fields due to the forcing. According to *Klein et al.* [2018], the six meteorological CCF fields with the biggest impact on low clouds are sea surface temperature (SST), estimated inversion strength (EIS), horizontal temperature advection (Tadv), 700 hPa pressure velocity (ω700), 700 hPa relative humidity (RH700), and wind speed (WS), with SST and EIS having considerably more influence than the others. Hence the change in low cloud radiative effect can be decomposed into a sum of six terms:

$$\Delta R = \frac{\partial R}{\partial SST}\Delta SST + \frac{\partial R}{\partial EIS}\Delta EIS + \frac{\partial R}{\partial Tadv}\Delta Tadv + \frac{\partial R}{\partial \omega 700}\Delta \omega 700 + \frac{\partial R}{\partial RH700}\Delta RH700 + \frac{\partial R}{\partial WS}\Delta WS. \tag{2}$$

In this study, we focus on low cloud adjustments, so ΔSST=0 and all other variables are taken from FixedSST experiments.

Meteorological Cloud Radiative Kernels

We use meteorological cloud radiative kernels ($\partial R/\partial x_i$) from *Myers et al.* [2021], as well as a new kernel for CESM2 that was not included in their analysis. These kernels were calculated from 20 (for CMIP5) or 50 years (for CMIP6) of a preindustrial control GCM simulation according to the method presented in *Scott et al.* [2020] and provide the GCM-simulated low cloud-induced change in TOA radiative flux per unit change in cloud-controlling factor x_i. Note that due to data limitations, the CESM2 meteorological cloud radiative kernel was calculated from 50 years of a historical simulation. These data are presented on a $5^\circ \times 5^\circ$ grid from 60°S-60°N and have units of W m $^{-2}$ dx_i^{-1}.

Meteorological Predictor Fields

We use monthly mean output from a control and an abrupt4xCO2 FixedSST experiment for CMIP5 (sstClim & sstClim4xCO2, respectively) and CMIP6 (piClim-control & piClim-4xCO2, respectively). We calculate Δx_i by taking the thirty-year average difference between the abrupt forcing run and the control run.

ω700, RH700, and WS are standard GCM outputs. Following *Scott et al.* [2020], EIS can be calculated from monthly mean GCM outputs as:

$$EIS = LTS - \Gamma_m^{850}(Z_{700} - Z_{LCL}), \tag{3}$$

where LTS is lower-tropospheric stability (the difference in potential temperature between 700 hPa and the surface), Γ_m^{850} is the moist-adiabatic lapse rate at 850 hPa, Z_{700} is the height of the 700 hPa pressure level relative to the surface, and Z_{LCL} is the height of the lifting condensation level relative to the surface.

Similarly, we follow *Scott et al.* [2020] to calculate Tadv as:

$$Tadv = -\frac{U_{10}}{a\cos(\phi)}\frac{\partial SST}{\partial \lambda} - \frac{V_{10}}{a}\frac{\partial SST}{\partial \phi}, \tag{4}$$

which uses a second-order centered finite-difference scheme where U_{10} and V_{10} are the zonal and meridional 10m wind components, ϕ is latitude, λ is longitude, and a is Earth's mean radius.

Note that the NCAR model does not output 10m wind components. As a work-around, we follow *Vimont et al.* [2009] and *Hwang and Chung* [2021] who estimate the 10m wind vectors by taking the average of the 1000 hPa and 850 hPa level winds and multiply it by 80%. In addition, near-surface wind speed is not output by CCSM4. Unfortunately the monthly average surface wind speed, found by taking the average of surface wind speeds at each time step over the course of the month, is not the same as taking the magnitude of the monthly average surface wind vector. Because WS is not a major driver of cloud adjustment [e.g. *Klein et al.* [2018] and results from other models below], we set the ΔWS term to NaN in our CCSM4 calculations and proceed.

Error Estimation

We calculate 95% uncertainty based on *Myers et al.* [2021]. At each grid box, we give the 95% confidence interval as,

$$\frac{\partial R}{\partial x_i}\Delta x_i \pm t\sqrt{\Delta \mathbf{x}_i^T C \Delta \mathbf{x}_i}\sqrt{\frac{N_{nom}}{N_{eff}}} = \frac{\partial R}{\partial x_i}\Delta x_i \pm \delta. \tag{5}$$

Above, C is the covariance matrix of regression coefficients at each grid cell from *Myers et al.* [2021]'s meteorological radiative kernels, $\Delta \mathbf{x}_i$ is a 7×1 vector of the six Δx_i values

and a one (note that we set the SST value to 0), and N_{nom}/N_{eff} is the ratio of the nominal to effective number of monthly values. For N_{nom}, we note that *Myers et al.* [2021] used data from July 1983-December 2018 and for N_{eff} we divide N_{nom} by 5 following *Myers et al.* [2021]'s rule of thumb that "we find that one out of five points is independent temporally." t is the critical value of the Student's t-test at the 95% significance level with $N_{eff} - 6$ degrees of freedom. Note that in *Myers et al.* [2021], they consider the critical t value for $N_{eff} - 7$ degrees of freedom, but because we remove SST from our analysis we consider only six.

This gives us an uncertainty at each grid cell. We calculate the global mean (denoted by angular brackets) error for each model (s) as,

$$\langle \frac{\partial R}{\partial x_i} \Delta x_i \rangle \pm \sqrt{\frac{\sum_k (\delta_k w_k)^2}{(\sum_k w_k)^2}} \sqrt{\frac{N^*_{nom}}{N^*_{eff}}} = \langle \frac{\partial R}{\partial x_i} \Delta x_i \rangle \pm s, \tag{6}$$

where δ_k is the uncertainty in the k-th grid box, w_k is the cosine of ϕ, and N^*_{nom}/N^*_{eff} is the ratio of nominal to effective number of $5^\circ \times 5^\circ$ grid boxes, taken here to be 30 per *Myers et al.* [2021]'s rule of thumb: "around 1 out of 30 grid boxes is independent."

Lastly, we take the global mean error for each model and calculate the multi-model mean error as,

$$s_{MMM} = \left(\sqrt{s_1^2 + \ldots + s_n^2} \right) / n, \tag{7}$$

where n is the number of models (in our case, six for CMIP5 and seven for CMIP6).

References

Hwang, Y.-T., and P.-C. Chung (2021), Seasonal Sensitivity of the Cross-Equatorial Hadley Cell Response to Extratropical Thermal Forcings, *Journal of Climate*, *34*, 3327–3342, doi:10.1175/JCLI-D-19-0938.1, publisher: American Meteorological Society Section: Journal of Climate.

Klein, S. A., A. Hall, J. R. Norris, and R. Pincus (2018), Low-Cloud Feedbacks from Cloud-Controlling Factors: A Review, in *Shallow Clouds, Water Vapor, Circulation, and Climate Sensitivity*, edited by R. Pincus, D. Winker, S. Bony, and B. Stevens, pp. 135–157, Springer International Publishing, Cham, doi:10.1007/978-3-319-77273-87.

Myers, T. A., R. C. Scott, M. D. Zelinka, S. A. Klein, J. R. Norris, and P. M. Pincus (2021), Observationa Constraints on Low-Cloud Feedback Reduce Uncertainty of Climate Sensitivity, *Nature Climate Change*, *11*, 501–507, doi:10.1038/s41558-021-01039-0.

Scott, R. C., T. A. Myers, J. R. Norris, M. D. Zelinka, S. A. Klein, M. Sun, and D. R. Doelling (2020), Observed Sensitivity of Low-Cloud Radiative Effects to Meteorological Perturbations over the Global Oceans, *Journal of Climate*, *33*(18), 7717–7734, doi:10.1175/JCLI-D-19-1028.1, publisher: American Meteorological Society Section: Journal of Climate.

Vimont, D. J., M. Alexander, and A. Fontaine (2009), Midlatitude Excitation of Tropical Variability in the Pacific: the Role of Thermodynamic Coupling and Seasonality, *Journal of Climate*, *22*, 518–534, doi:10.1175/2008JCLI2220.1, publisher: American Meteorological Society Section: Journal of Climate.

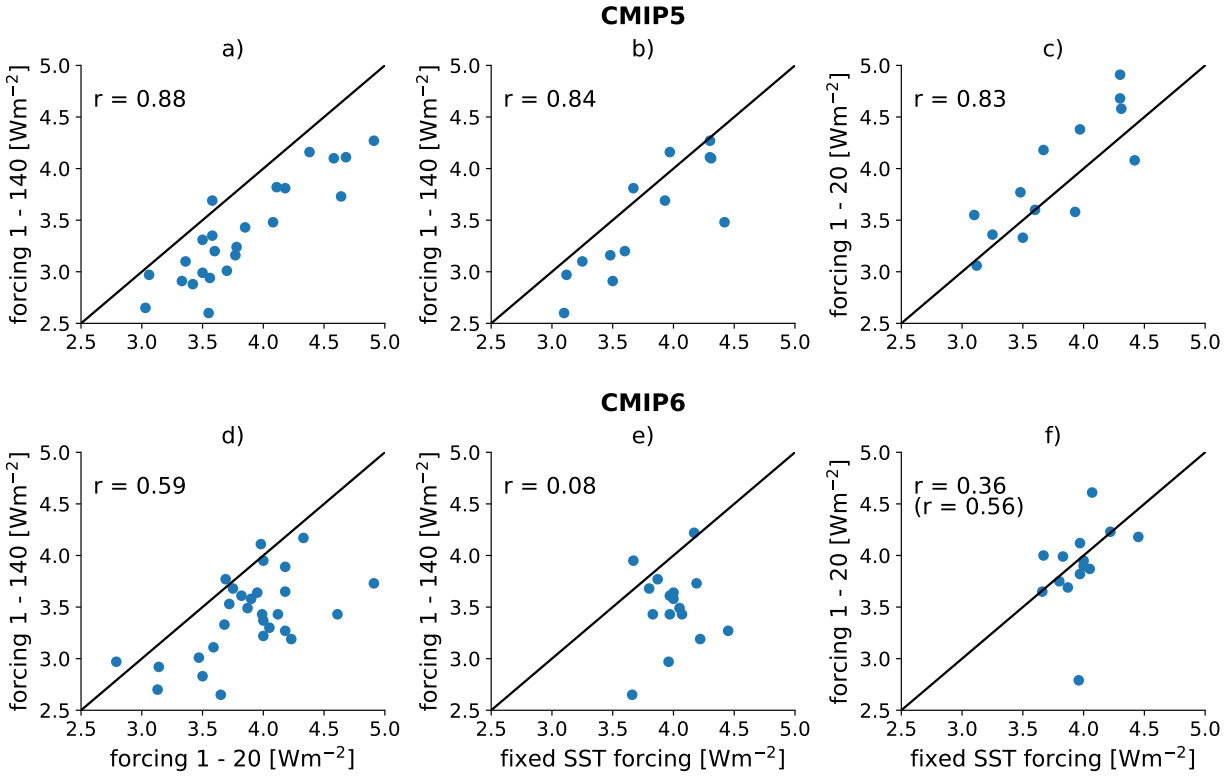

Figure S1. Comparisons of different methods of estimating radiative forcing in CMIP5 and CMIP6. a) F_{1-140} versus F_{1-20} in CMIP5, b) F_{1-140} versus F_{fix} in CMIP5, c) F_{1-20} versus F_{fix} in CMIP5, d) F_{1-140} versus F_{1-20} in CMIP6, e) F_{1-140} versus F_{fix} in CMIP6, f) F_{1-20} versus F_{fix} in CMIP6. In all panels the Pearson correlation coefficient r is shown in the upper left and the black lines show the 1:1 line. The text in brackets in panel f) gives the Pearson correlation coefficient when CNRM-ESM2.1 (the outlier with anomalously small F_{1-20}) is excluded from the correlation.

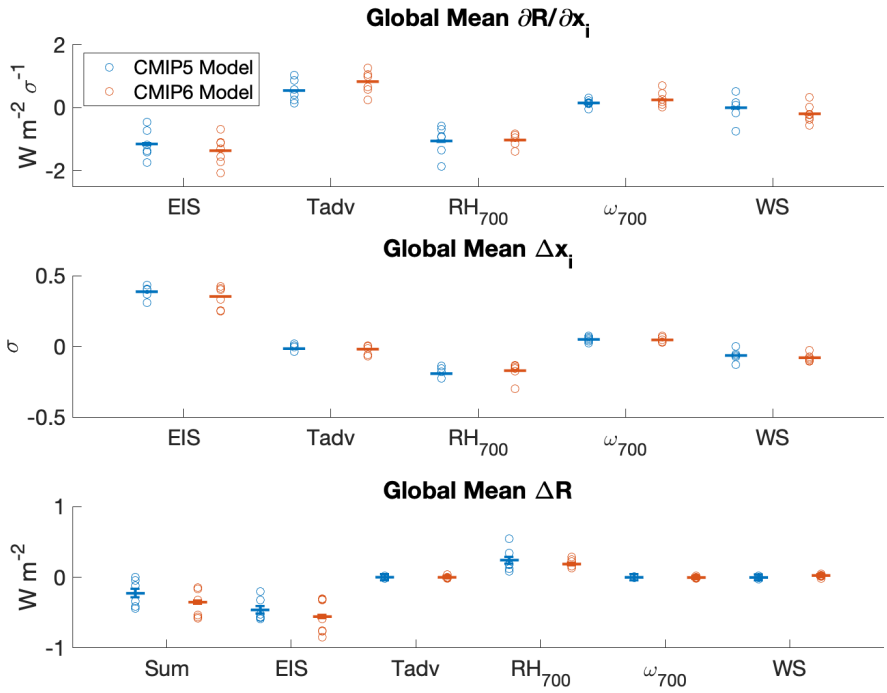

Figure S2. Results of the CCF analysis. The top panel show the global-mean values of the meteorological cloud radiative kernels for the CMIP5 and CMIP6 models (blue and red circles, respectively), which demonstrates how the sensitivity of the CRE R to the meteorological controling factors varies between the model generations. The middle panel shows the global-mean responses of the meteorological controling factors to quadrupling of CO_2, in units of per standard deviation. The bottom panel shows the total change in CRE ΔR estimated from the CCF analysis ("Sum"), as well as the contributions from the individual CCF fields. The error bars show the multimodel mean error.